PNAS RESEARCH ARTICLE | BIOCHEMISTRY

PRL-1/2 phosphatases control TRPM7 magnesium-dependent function to regulate cellular bioenergetics

Serge Hardy[a,b], Yevgen Zolotarov[a,b], Jacob Coleman[a,b], Simon Roitman[a,b], Hira Khursheed[a,b], Isabelle Aubry[a,b], Noriko Uetani[a,b], and Michel L. Tremblay[a,b,1]

Edited by Michael Lenardo, NIH, Bethesda, MD; received December 12, 2022; accepted March 3, 2023

Phosphatases of regenerating liver (PRL-1, PRL-2, PRL-3; also known as PTP4A1, PTP4A2, PTP4A3, respectively) control intracellular magnesium levels by interacting with the CNNM magnesium transport regulators. Still, the exact mechanism governing magnesium transport by this protein complex is not well understood. Herein, we have developed a genetically encoded intracellular magnesium-specific reporter and demonstrate that the CNNM family inhibits the function of the TRPM7 magnesium channel. We show that the small GTPase ARL15 increases CNNM3/TRPM7 protein complex formation to reduce TRPM7 activity. Conversely, PRL-2 overexpression counteracts ARL15 binding to CNNM3 and enhances the function of TRPM7 by preventing the interaction between CNNM3 and TRPM7. Moreover, while TRPM7-induced cell signaling is promoted by PRL-1/2, it is reduced when CNNM3 is overexpressed. Lowering cellular magnesium levels reduces the interaction of CNNM3 with TRPM7 in a PRL-dependent manner, whereby knockdown of PRL-1/2 restores the protein complex formation. Cotargeting of TRPM7 and PRL-1/2 alters mitochondrial function and sensitizes cells to metabolic stress induced by magnesium depletion. These findings reveal the dynamic regulation of TRPM7 function in response to PRL-1/2 levels, to coordinate magnesium transport and reprogram cellular metabolism.

PRL phosphatase | magnesium | TRPM7 | metabolism | magnesium sensor

Phosphatases of regenerating liver (PRL-1, PRL-2, PRL-3; also known as PTP4A1, PTP4A2, PTP4A3, respectively) have been associated with the progression of multiple cancer types (1, 2) and the control of magnesium homeostasis through an interaction with the Cyclin and CBS Domain Divalent Metal Cation Transport Mediator (CNNM) family in a substrate-independent manner (3, 4). This family has four highly conserved members in mammals, which have different tissue distribution (5, 6) and genetic defects of CNNM2 and 4 have been linked to hypomagnesemia (7, 8). The PRL-1,2,3/CNNM1-4 complex has been well characterized whereby either PRL knockdown or disruption of complex formation reduces intracellular magnesium levels (3, 4, 9, 10). Modulating intracellular magnesium levels correlates with a rapid change in PRL-1/2 expression through an evolutionarily conserved upstream open-reading frame present in their 5′ untranslated mRNA region (11). Some of the PRL-2/3 proto-oncogenic activity is linked to their interaction with CNNM3/4, which affects both magnesium flux and tumor growth (3, 4, 9, 10). It is unclear whether the CNNMs are magnesium transporters or transport mediators (12–14). More recently, all CNNMs were shown to interact with TRPM7 (15, 16), a ubiquitously expressed divalent cation channel which is predominantly involved in the influx of magnesium, calcium, and zinc (17). Nonetheless, the exact regulatory role of the PRLs in this protein complex is still unclear.

TRPM7 is required for proper development and magnesium homeostasis (18–21). TRPM7 and its homolog, TRPM6, are unique among the TRP family of channels in that they contain a serine/threonine kinase in the C-terminal region of the protein (17). Nuclear translocation of the cleaved kinase domain was shown to phosphorylate histones and regulate gene expression (22). Although TRPM7 is present at the plasma membrane, the majority is located in unique intracellular vesicles (23, 24). TRPM7 is involved in cellular proliferation and migration and has been linked to cancer progression (25, 26). It also regulates intravasation by affecting the sensitivity of tumor cells to shear stress (27, 28). As with PRL-1/2, TRPM7 mRNA translation rapidly increases under magnesium-limiting conditions (29). Its function is also regulated by intracellular magnesium levels, where channel activity is inversely correlated with magnesium levels (30–32). However, the mechanism behind this specific aspect of TRPM7 function is not well understood.

Intracellular magnesium content is tightly regulated and is required for energy production either indirectly as a part of the Mg-ATP complex or directly as a cofactor for many metabolic enzymes involved in mitochondrial respiration and glycolysis (33).

Significance

Expression of the phosphatases of regenerative liver-1/2 (PRL-1/2) is controlled by intracellular magnesium using a mechanism involving an evolutionarily conserved 5′untranslated mRNA region. TRPM7 is the main magnesium transporter in vertebrates and its activity is regulated by various stimuli (i.e., magnesium itself, Mg-ATP, pH, PIP2), but the recent identification of intrinsic molecular interactors, including the PRL-1/2 binding partners CNNMs, has broadened our understanding of cellular magnesium transport. Our study uncovers a mode of regulation of magnesium transport where PRL-1/2 act as magnesium biosensors controlling the CNNM3/TRPM7 interaction, to dictate TRPM7 signaling and regulate energy-sensing pathways. This magnesium-dependent mechanism affecting TRPM7 function is thus fundamental for the role of PRL in oncogenesis and cellular bioenergetics.

Author contributions: S.H., Y.Z., J.C., I.A., N.U., and M.L.T. designed research; S.H., Y.Z., J.C., S.R., H.K., I.A., and N.U. performed research; S.H., Y.Z., J.C., S.R., H.K., I.A., and N.U. analyzed data; and S.H., Y.Z., and M.L.T. wrote the paper.

The authors declare no competing interest.

This article is a PNAS Direct Submission.

[1]To whom correspondence may be addressed. Email: michel.tremblay@mcgill.ca.

This article contains supporting information online at https://www.pnas.org/lookup/suppl/doi:10.1073/pnas.2221083120/-/DCSupplemental.

Published March 27, 2023.

Lactate, the end product of glycolysis, is an agonist of intracellular magnesium flux by inducing its rapid release from endoplasmic reticulum stores, to facilitate mitochondrial uptake, and ultimately controls cellular metabolism (34). Interestingly, magnesium-dependent changes in PRL-2 expression also contribute to the metabolic rewiring of cells (11) and ATP turnover decreases in cells isolated from PRL-2-/- animals (35), suggesting a pivotal regulatory role of the PRL/CNNM protein complex in these processes.

Herein, using a genetically encoded intracellular magnesium reporter, we demonstrate that the CNNM family inhibits TRPM7 function in a magnesium-dependent manner. Moreover, we elucidate the role of PRL-1/2 in controlling the dynamic interplay of the TRPM7/CNNM3 protein complex in magnesium transport, cell signaling, and metabolism.

Results

Development of a First-Generation Magnesium Biosensor to Assess TRPM7 Function. The expression of PRL-1/2 was recently shown to be controlled by a highly conserved region within the mRNA 5′UTR (untranslated region) (11). This regulatory element acts as a sensor of intracellular magnesium levels allowing PRL translation to occur under low magnesium conditions and inhibiting it when abundant. We used the magnesium-sensing ability of the PRL-2 5′UTR to develop a real-time translation-based magnesium reporter, which is an innovation in the study of intracellular magnesium dynamics. To this end, we designed a first-generation magnesium reporter by fusing the PRL-2 5′UTR to the engineered firefly luciferase (Fluc) gene *luc2* (UTR Luc) (Fig. 1*A* and *SI Appendix*, Fig. S1*A*). In addition,

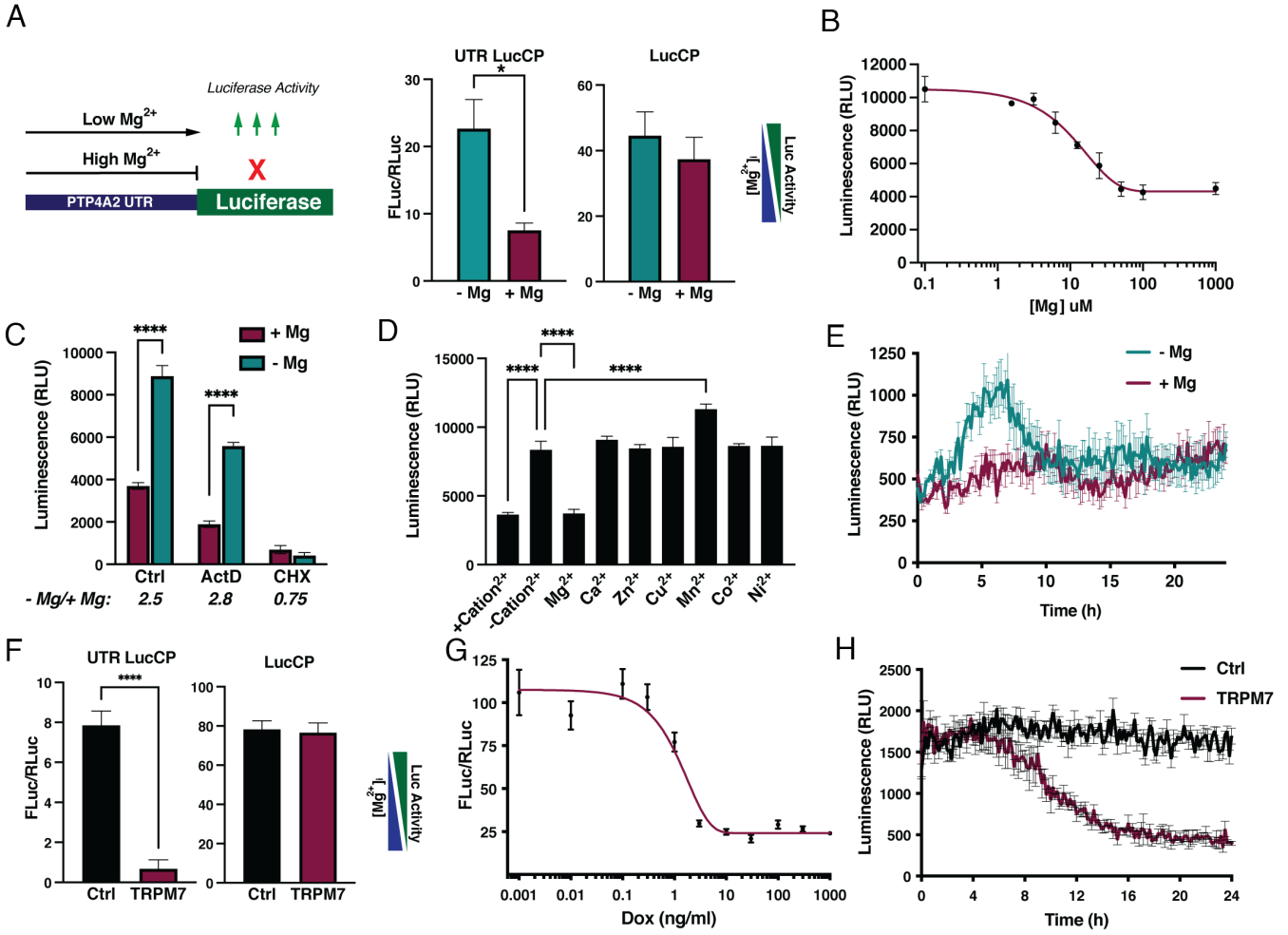

Fig. 1. Development of a first-generation magnesium biosensor to evaluate TRPM7 function. (*A*) PRL-2 UTR luciferase reporter constructs with a destabilizing sequence CP (LucCP) used to detect luminescence changes in response to magnesium levels. HEK293 cells were transfected with the UTR LucCP reporter and Renilla luciferase control constructs, treated for 24 h in the presence or absence of 1 mM magnesium followed by luciferase activity measurements. Plot is representative of three independent experiments. Data are means ± SD (n = 4); **P* < 0.05 by one-way ANOVA. (*B*) HeLa cells stably expressing the UTR LucCP reporter construct were incubated for 6 h with various magnesium concentrations followed by luciferase activity measurements. Data are means ± SD (n = 4). (*C*) HeLa cells stably expressing the UTR LucCP reporter construct were incubated for 6 h in the presence or absence of magnesium with or without the indicated inhibitors followed by luciferase activity measurements. ActD: Actinomycin D (1 μg/mL); CHX: Cycloheximide (50 μg/mL). Plot is representative of two independent experiments. Data are means ± SD (n = 4); *****P* < 0.0001 by two-way ANOVA. (*D*) HeLa cells stably expressing the UTR LucCP reporter construct were incubated for 6 h in either the presence of all the indicated cations (+cations^{2+}) or in the absence of −cations^{2+} and replenished with the individual cations. Plot is representative of three independent experiments. Data are means ± SD (n = 4); *****P* < 0.0001 by two-way ANOVA. (*E*) Real-time bioluminescence assay using HeLa cells stably expressing the UTR LucCP reporter construct incubated in the presence and absence of magnesium. (*F*) HEK293 dox-inducible TRPM7 cells were transfected with the UTR LucCP reporter and Renilla luciferase control constructs, treated for 24 h with dox (1 μg/mL) followed by luciferase activity measurements. Plot is representative of three independent experiments. Data are means ± SD (n = 4); *****P* < 0.0001 by one-way ANOVA. (*G*) HEK293 dox-inducible TRPM7 cells stably expressing the UTR LucCP reporter construct were treated for 24 h with various Dox concentration followed by luciferase activity measurements. Data are means ± SD (n = 4). (*H*) Real-time bioluminescence assay using HEK293 dox-inducible TRPM7 cells stably expressing the UTR LucCP reporter construct incubated in the presence and absence of Dox (1 μg/mL).

we introduced a destabilized sequence to the *luc2* gene (UTR LucCP) which decreases the protein half-life to provide greater temporal resolution and the ability to detect rapid changes in intracellular magnesium. To validate our system, we transfected these constructs into both HeLa and HEK293 cells and assessed whether the presence of the UTR and destabilized LucCP sequence reduces luciferase activity (*SI Appendix*, Fig. S1*B*). We observed a significant induction of luminescence after 6 h of magnesium deprivation in HeLa cells expressing only the UTR-based reporters (Fig. 1*A* and *SI Appendix*, Fig. S1*C*). HeLa cells stably expressing the UTR LucCP reporter construct showed a rapid increase in luciferase activity following magnesium withdrawal that peaked around 6 h, followed by reduction of luciferase activity back to the level observed in the presence of magnesium (*SI Appendix*, Fig. S1*D*). Importantly, the luciferase signal of this new reporter is dose dependent on magnesium, with resolution in the range of 1 to 100 μM extracellular magnesium (Fig. 1*B*), which also corresponds to reported concentrations' modulating activity of the magnesium transporter TRPM7 (36). To validate that the observed response is in fact driven by mRNA translation, transcription was inhibited using actinomycin D and luciferase activity was still induced following magnesium depletion. As expected, treatment with the mRNA translation inhibitor cycloheximide resulted in a loss of induction (Fig. 1*C*), confirming a posttranscriptional regulation by magnesium as previously described (11).

We next evaluated the specificity of the reporter by modulating other divalent cations present in cell culture media (Fig. 1*D*). In response to cation depletion, which induces an increase in luminescence, only the presence of magnesium was able to restore the signal to that of the control (all divalent cations present). Also, we observed an increase in luminescence in the presence of manganese, which can occupy magnesium-binding sites present in various proteins. Moreover, increasing levels of extracellular calcium and zinc, two other divalent cations transported by TRPM7, do not affect luminescence (*SI Appendix*, Fig. S2*A*). To further assess the specificity of the reporter, cells were treated with carbonyl cyanide-4-(trifluoromethoxy)-phenylhydrazone (FCCP), which induces magnesium release from the mitochondria to the cytosol (37, 38). In the presence or absence of extracellular magnesium, we observed a significant decrease in reporter activity upon FCCP treatment, suggesting a rise in cytosolic magnesium (*SI Appendix*, Fig. S2*B*). Finally, we evaluated the possibility of using stable HeLa (UTR LucCP) cells in a real-time bioluminescence assay. Interestingly, a rapid increase in luminescence is observed under low magnesium with a peak at approximately 6 h (Fig. 1*E*). This rapid increase in luminescence is quickly balanced back to the levels observed in normal magnesium conditions, under which a similar modulation was not observed.

We next assessed the consequence of increasing intracellular magnesium on the UTR LucCP reporter. To this end, we overexpressed TRPM7 using the well-characterized HEK293 doxycycline (dox)-inducible system (39) to trigger an increase in intracellular magnesium levels (*SI Appendix*, Fig. S3*A*). We transfected the UTR-based and control reporters into the inducible TRPM7 cells, treated them with dox, and measured luciferase activity. We observed a robust drop of luciferase activity upon induction of TRPM7 expression, with the most pronounced effect using the UTR LucCP reporter construct (Fig. 1*F* and *SI Appendix*, Fig. S3*B*). Conversely, TRPM7 induction does not significantly affect luciferase activity in the absence of the UTR. We then generated HEK293 dox-inducible TRPM7 cells stably expressing the UTR LucCP reporter construct that showed both a dose-dependent (Fig. 1*G*) and time-dependent (*SI Appendix*, Fig. S3*C*) decrease in luminescence following TRPM7 overexpression. Similarly, in a real-time bioluminescence assay, TRPM7 induction provoked a reduction in luminescence over time (Fig. 1*H*).

Overall, using the magnesium-sensitive PRL-2 UTR, we have developed a translationally regulated luciferase-based intracellular magnesium reporter system. Importantly, this reporter is specific to magnesium, a common limitation of traditional chelator-based reporters, and can be used to study magnesium modulation in real-time live-cell bioluminescence assays.

TRPM7 Function Is Negatively Regulated by the CNNM3/ARL15 Complex. TRPM7 patch-clamp recording is mostly limited to the plasma membrane, which might not represent the entire functional activity of this chanzyme as it is mostly localized to intracellular vesicles (23, 24). As such, we used our reporter system to characterize potential regulators of TRPM7 overall function. The BioID experiment performed in our previous studies indicated that the small GTPase ARL15 not only interacts with all CNNM members to mediate magnesium flux (40), but TRPM7 as well, which suggests the formation of a tertiary multiprotein complex. Subsequent studies confirmed that all CNNMs directly bind TRPM7 (15, 16), and ARL15 overexpression decreases TRPM7-mediated current (16). Thus, we first evaluated this association in the HEK293 dox-inducible TRPM7 cells stably expressing the UTR LucCP reporter. To study the interaction between CNNM3, ARL15, and TRPM7, we performed coimmunoprecipitation (co-IP) experiments with these overexpressed proteins (Fig. 2*A*). Western blot analysis confirmed the association of CNNM3 with TRPM7. Interestingly, the presence of ARL15 significantly promoted this interaction. To determine whether the observed effect extends to all the four members of the CNNM family, we performed co-IPs of TRPM7, ARL15, and CNNM1-4 (*SI Appendix*, Fig. S4*A*). As with CNNM3, ARL15 enhanced the interaction between TRPM7 and all other CNNMs.

Since TRPM7 contains a C-terminal kinase domain (32, 41), we examined the potential involvement of this feature in the interaction with CNNMs. To this end, either dox-inducible WT TRPM7 or a kinase-dead mutant (K1646R) was transfected into HEK293 cells along with ARL15 and CNNM3. Co-IP revealed that the interaction between TRPM7, CNNM3, and ARL15 is independent of kinase activity (*SI Appendix*, Fig. S4*B*). This is consistent with previous studies which showed that kinase-dead TRPM7 does not affect magnesium homeostasis (18, 39). We next performed a reporter assay to assess the potential roles of CNNMs and ARL15 on TRPM7 function. Once again, TRPM7 overexpression mediated an increase in intracellular magnesium content, as determined by a dramatic decrease in luminescence, and coexpression of CNNMs partially inhibited this TRPM7 function (Fig. 2*B*). Importantly, a similar effect was observed using NS8593 (*SI Appendix*, Fig. S5), a magnesium-dependent TRPM7 channel inhibitor (42). Moreover, although the expression of ARL15 alone had no effect on TRPM7 function, we observed a synergistic effect of ARL15 and CNNM3 on TRPM7 inhibition (Fig. 2*C*). Taken together, the data provide evidence of a multiprotein complex involving TRPM7, CNNMs, and ARL15, which serves to inhibit TRPM7-mediated magnesium transport.

It was previously shown that TRPM7 plays a role in cell morphology and cytoskeletal rearrangement. TRPM7 overexpression results in rounding of cells and decreased lamellipodia formation (32, 43). To confirm previous reports, we induced TRPM7 overexpression in HEK293 cells using dox and observed cell rounding in addition to decreased confluency as compared to cells with endogenous TRPM7 expression (Fig. 2 *D* and *E*). Importantly, cell number was not affected by TRPM7 overexpression (*SI Appendix*, Fig. S6*A*). Overexpression of

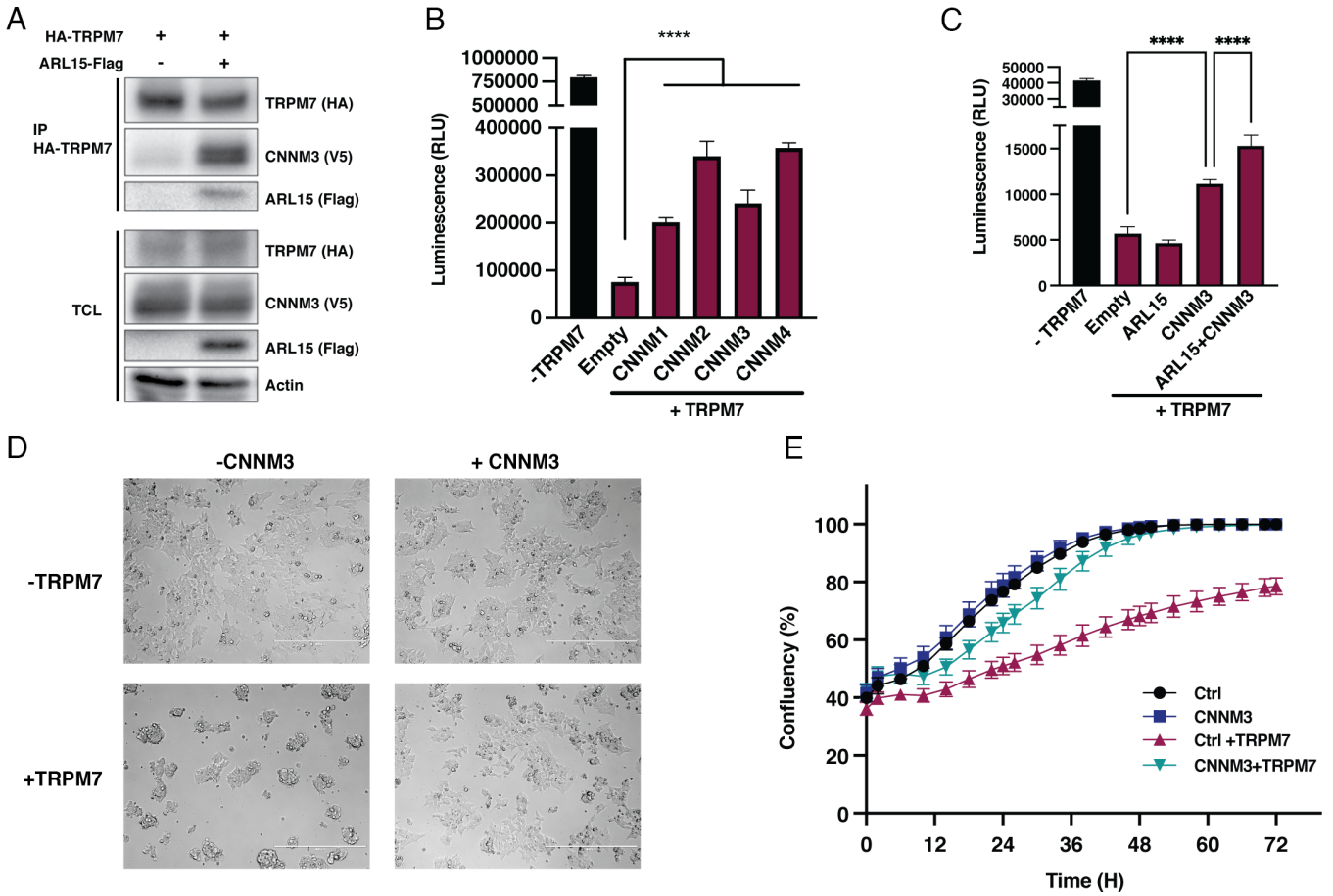

Fig. 2. TRPM7 function is negatively regulated by CNNMs. (*A*) HEK293 dox-induced HA-TRPM7 cells were transfected with CNNM3-V5 in the absence or presence of ARL15-Flag. HA-TRPM7 was immunoprecipitated (IP) and immunoblotted with Flag and V5 antibodies. TCL: Total cell lysate. (*B*) HEK293 dox-inducible HA-TRPM7 cells stably expressing the UTR LucCP reporter construct were transfected with empty control or CNNM1-4-Flag and treated for 24 h with dox followed by luciferase activity measurements. Plot is representative of four independent experiments. Data are means ± SD (n = 4); ****$P < 0.0001$ by two-way ANOVA. (*C*) HEK293 dox-inducible HA-TRPM7 cells stably expressing the UTR LucCP reporter construct cells were transfected with empty control, CNNM3-Flag, and ARL15-V5 and treated for 24 h with dox followed by luciferase activity measurements. Plot is representative of three independent experiments. Data are means ± SD (n = 4); ****$P < 0.0001$ by two-way ANOVA. (*D*) Representative pictures of HEK293 dox-inducible HA-TRPM7 cells transfected at low density with empty control or CNNM3-Flag and treated for 48 h with dox. (*E*) Real-time confluency of HEK293 dox-inducible HA-TRPM7 cells transfected at low density with empty control or CNNM3-Flag and treated for 72 h with dox.

CNNM3 alone did not significantly affect morphology. However, overexpression of either CNNM3 or other CNNMs restored TRPM7-mediated changes in cell morphology and confluency (Fig. 2*E* and *SI Appendix*, Fig. S6*B*). Only TRPM7-expressing control cells lacking CNNM overexpression were unable to reach complete confluency. Moreover, coover-expression of CNNMs and TRPM7 allowed them to become confluent at the same rate as endogenous control cells. These results corroborate the inhibitory effect of the CNNMs on TRPM7-mediated function.

PRL-1/2 Promotes TRPM7 Function via Their Interaction with CNNM3. The PRL phosphatases were previously shown to interact with CNNMs and affect magnesium homeostasis (3, 4). Additionally, intracellular magnesium levels regulate PRL-1/2 mRNA translation (11), where low $[Mg^{2+}]_i$ promotes high PRL expression (Fig. 3*A*). To assess potential PRL-1/2 function within the complex, TRPM7, CNNM3, and ARL15 were individually overexpressed in HEK293 cells and PRL-1/2 expression was evaluated by western blot analysis. Interestingly, we observed that either CNNMs or ARL15 overexpression increases PRL-1/2 expression, whereas TRPM7 decreases it (Fig. 3*A* and *SI Appendix*, Fig. S7). Moreover, among all divalent cations reported to be transported by TRPM7, only magnesium modulated PRL-1/2 expression (Fig. 3*B*). Using our luciferase-based intracellular magnesium reporter system, we observed that CNNM3 overexpression reduces intracellular magnesium levels, whereas PRL-2 has the opposite effect (*SI Appendix*, Fig. S8*A*). In addition, overexpression of PRL-2 D69A or CNNM3 D426A, which blocks PRL-2/CNNM3 complex formation (3, 9), did not affect intracellular magnesium levels. Thus, we postulate that PRL-2 may play a regulatory role in TRPM7-dependent magnesium transport via its association with the CNNM3.

To assess the putative role of PRL-2 in CNNM3-mediated inhibition of TRPM7 activity, we performed a co-IP experiment whereby HA-TRPM7 was coexpressed with CNNM3 and PRL2. Following HA-TRPM7 immunoprecipitation, we observed that PRL-2 overexpression reduces the association between CNNM3 and TRPM7 (Fig. 3*C*). To assess the effect of PRL-2 on TRPM7 activity, we performed a magnesium reporter assay whereby PRL-2 was expressed in either the presence or absence of overexpressed CNNM3. As described above, the TRPM7-driven increase in magnesium content strongly reduces luminescence, an effect which is counteracted by CNNM3 (Fig. 3*D*). Interestingly, PRL-2 could partially restore TRPM7 function in the presence of CNNM3, presumably by reducing the inhibitory effect of

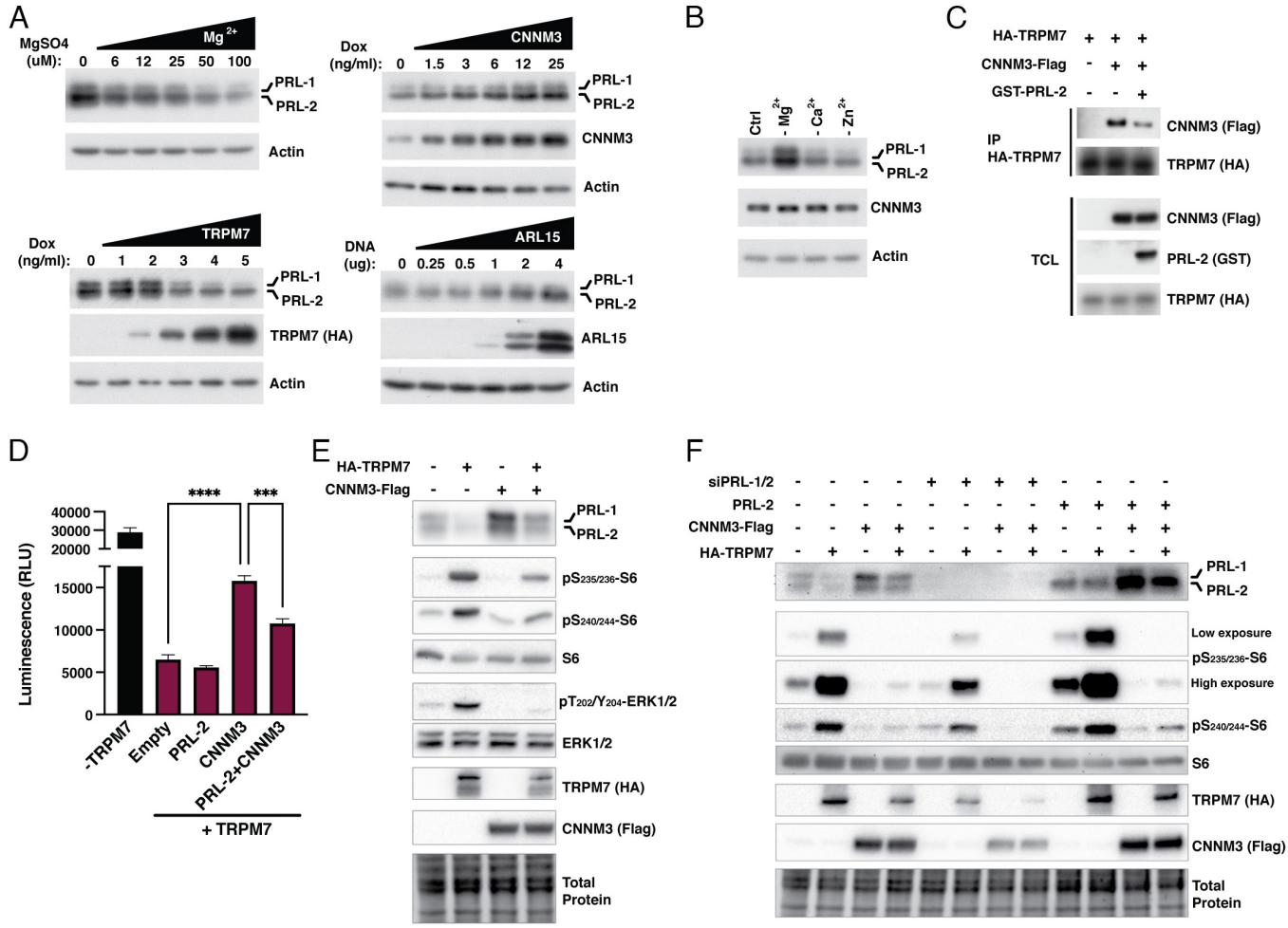

Fig. 3. PRL-1/2 promotes TRPM7 magnesium-dependent function and signaling. (*A*) Western blot analysis of PRL-1/2 expression in HEK293 cells using various magnesium concentrations, following overexpression of TRPM7 or CNNM3 using Dox-inducible HEK293 cells, or transfection of ARL15-Flag. (*B*) Western blot analysis of HEK293 dox-inducible HA-TRPM7 cells treated for 6 h in the absence of magnesium or calcium or treated with the zinc chelator TPEN (10 μM). (*C*) HEK293 dox-induced HA-TRPM7 cells were transfected with CNNM3-Flag in the absence or presence of GST-PRL-2. HA-TRPM7 was immunoprecipitated (IP) and immunoblotted with Flag and GST antibodies. TCL: Total cell lysate. (*D*) HEK293 dox-inducible HA-TRPM7 cells stably expressing the UTR LucCP reporter construct were transfected with empty control, CNNM3-Flag, or GST-PRL-2 and treated for 24 h with dox followed by luciferase activity measurements. Plot is representative of three independent experiments. Data are means ± SD (n = 4); ****$P < 0.0001$ by two-way ANOVA. (*E* and *F*) HEK293 dox-inducible HA-TRPM7 cells were transfected with (*E*) control Green Fluorescent Protein (GFP) or CNNM3-Flag followed by 24 h Dox treatment, or cells were first transfected with (*F*) control or PRL-1/2-targetting small interfering RNAs (siRNAs) for 24 h, then with control (GFP), CNNM3-Flag, or PRL-2 followed by 24 h Dox treatment.

CNNM3 on TRPM7. We also observed that PRL-2 overexpression affects the localization of a pool of plasma membrane CNNM3 proteins to the cytoplasm (*SI Appendix*, Fig. S8*B*), although this effect was not observed with the CNNM3 D426A mutant that is unable to bind the PRLs (9), suggesting that trafficking of the PRL-2/CNNM3 protein complex could be involved in regulating magnesium transport.

To gain further mechanistic insight on the observed TRPM7 inhibition, we examined the effect of CNNM3 on TRPM7-mediated downstream signaling. As shown above, PRL-1/2 expression is sensitive to intracellular magnesium levels and can be independently modulated by TRPM7 and CNNM (Fig. 3*A*). We further show that CNNM3 counteracts the TRPM7-induced downregulation of PRL-1/2 expression (Fig. 3*E*). TRPM7 has been linked with mTORC1 (mechanistic target of rapamycin complex 1) activation in lymphocytes, where TRPM7 knockout resulted in delayed mTORC1 signaling as observed by phosphorylation of the p70 ribosomal protein S6 kinase (S6K) (44). In response to TRPM7 overexpression, we observe ribosomal protein S6 (S6) hyperphosphorylation at S240/S244 (Fig. 3*E*). In addition, S6 is also hyperphosphorylated at S235/S236, which are also target sites of the p90 ribosomal protein S6K (RSK). We also observed that, while overexpression of CNNM3 alone does not affect S6 phosphorylation, it counteracts the hyperphosphorylation induced by TRPM7 when both proteins are overexpressed. ERK-1/2 activity, which is upstream of RSK, follows a pattern of phosphorylation similar to S6. In line with these findings, using the TRPM7 inhibitor NS8593, we observed a decrease in mTORC1-dependent signaling and synergy with CNNM3 to reduce TRPM7 signaling (*SI Appendix*, Fig. S9).

Since CNNM3 has an antagonistic effect on TRPM7 signaling, we sought to understand the effect of PRL-1/2 on TRPM7 signaling by modulating their expression. When both PRL-1 and PRL-2 were knocked down using siRNA, the effect of TRPM7 on S6 phosphorylation was dampened (Fig. 3*F*). On the contrary, PRL-2 overexpression has the opposite effect, with increased S6 phosphorylation as compared to endogenous levels (Fig. 3*F*). These findings suggest that the interaction of CNNM3 with PRL-1/2 prevents the observed antagonism of TRPM7 by CNNM3.

TRPM7 activity is regulated by intra- and extracellular magnesium levels (30–32), but the regulatory mechanism of action is

not well understood. Moreover, the native TRPM7 channel is inhibited by extracellular magnesium in a manner similar to the dose–response effect we observed for PRL-1/2 mRNA translation [Fig. 3*A* and (36)], where low levels of magnesium lead to higher TRPM7 activity and higher PRL-1/2 expression. Given that most studies involving TRPM7 are performed in overexpressed systems, we performed co-IP experiments under low and normal magnesium for four hours in uninduced HEK293 TRPM7 cells, which keep HA-TRPM7 protein levels as low as possible. When TRPM7 was immunoprecipitated (IP), less CNNM3 was detected under low magnesium as compared to more physiological levels (Fig. 4*A*). Similarly, when IP of CNNM3 was performed, its interaction with TRPM7 was reduced in low magnesium (*SI Appendix*, Fig. S10*A*). Immunoprecipitation of native TRPM7 in MCF-7 cells incubated in low magnesium also shows a similar pattern of protein complex formation (*SI Appendix*, Fig. S10*B*).

Considering that we previously established that CNNM3 plays an inhibitory role in TRPM7 function, we hypothesized that decreasing the interaction between TRPM7 and CNNM3 under low magnesium conditions could promote magnesium influx. In line with this, when CNNM3 is IP under low magnesium, we observed an increased interaction with PRL-1/2 coupled to a decreased association with TRPM7 (Fig. 4*B*). This is consistent with a model where PRL-1/2 mRNA translation is rapidly up-regulated upon magnesium depletion to bind CNNM3 and release TRPM7 from CNNM3-mediated inhibition to promote its activity. To directly test this model, we blocked protein synthesis using cycloheximide (CHX) under low magnesium conditions to prevent PRL-1/2 upregulation and observed sustained association between CNNM3 and TRPM7 (Fig. 4*C*). Moreover, siRNA-mediated depletion of PRL-1/2 similarly stabilizes the interaction between CNNM3 and TRPM7 despite lowering magnesium levels (Fig. 4*D*). ARL15, which we show strengthens the interaction between CNNM3 and TRPM7 (Fig. 2*A*), interacts less with CNNM3 upon magnesium depletion (*SI Appendix*, Fig. S10*B*). Since these results suggest competition between PRL-1/2 and ARL15 for CNNM3 binding, we overexpressed ARL15, CNNM3, and increasing amounts of PRL-2 to study protein complex formation. Upon CNNM3 immunoprecipitation, we observed that as association with PRL-2 increases, that with ARL15 decreases (*SI Appendix*, Fig. S11*A*). However, it also appears that PRL-2 overexpression can impact ARL15 expression, suggesting that ARL15 protein stability is reduced when not in complex with CNNM3. To test this hypothesis, we overexpressed ARL15 alone and with either CNNM3 or MG132, a proteasomal degradation inhibitor (*SI Appendix*, Fig. S11*B*). Overexpression of CNNM3 had a similar effect as MG132 on ARL15 levels, suggesting that the presence of CNNM3 prevents ARL15 degradation. Overall, a dynamic interplay emerges where the interaction between CNNM3 and TRPM7 is regulated by PRL-1/2 and ARL15 in response to changes in magnesium. In addition, these data reveal a major regulatory role of PRL-1/2 in the control of TRPM7 activity.

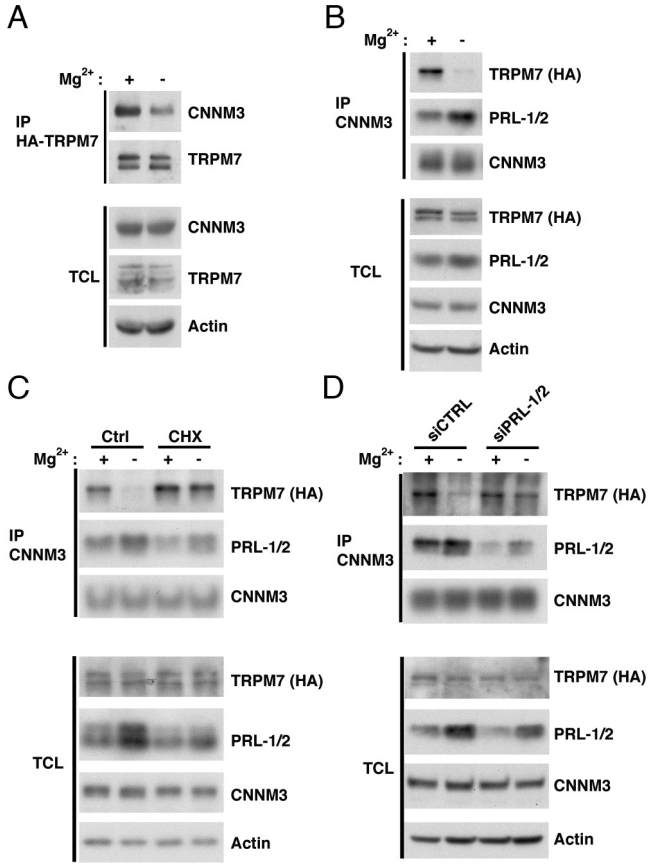

Fig. 4. Endogenous PRL-1/2 reduces CNNM3 interaction with TRPM7 following magnesium depletion. (*A* and *B*) Uninduced HEK293 dox-inducible HA-TRPM7 cells were incubated with and without 1 mM magnesium for 4 h followed by TRPM7 (*A*) or CNNM3 (*B*) immunoprecipitation (IP). (*C*) Uninduced HEK293 dox-inducible HA-TRPM7 cells were incubated with and without 1 mM magnesium for 4 h in the absence or presence of cycloheximide (CHX) followed by CNNM3 immunoprecipitation. (*D*) Uninduced HEK293 dox-inducible HA-TRPM7 cells were transfected with control or PRL-1/2-targetting siRNAs for 48 h. CNNM3 was immunoprecipitated following 4 h magnesium depletion.

TRPM7 and PRL-1/2 Synergize to Maintain Cellular Bioenergetics. Decreased intracellular magnesium leads to reduced ATP levels since this nucleotide must bind magnesium to be biologically active and is therefore commonly referred to as Mg-ATP (45). In addition, ATP depletion due to changes in extracellular magnesium levels can lead to an increase in AMP-activated protein kinase (AMPK) activity in the MCF-7 human breast cancer cell line (11) where the PRLs have important oncogenic functions (46, 47). As such, we opted to use this cell line as a biological system to study the effect of PRL-1/2 and TRPM7 modulation on cellular bioenergetics. Given that endogenous TRPM7 is expressed at very low levels in most cell types, we used a rabbit antibody for immunoprecipitation followed by western blot with a mouse antibody to avoid antibody cross-reaction (22, 48). Of note, TRPM7 is cleaved (22) and tends to oligomerize on SDS-PAGE which could explain why three bands are visible. Interestingly, targeting endogenous PRL-1/2 and/or TRPM7 using siRNAs in MCF-7 cells resulted in increased AMPK activity (Fig. 5*A*). We also observed a compensatory feedback mechanism where the expression of TRPM7 is higher in the absence of PRL-1/2 and vice versa.

Given the importance of magnesium in metabolism and mitochondrial ATP production, we performed a Seahorse flux assay where we observe significantly dysregulated mitochondrial function in PRL-1/2 targeted cells where a decline of ATP production, mitochondrial respiration, and mitochondrial energy reserve (spare respiratory capacity) was detected (Fig. 5*B*). While TRPM7 depletion alone shows no effect, knockdown of PRL-1/2 in conjunction with TRPM7 produces a synergistic effect on the mitochondrial function. We then measured glycolytic function under similar conditions described above to demonstrate that targeting both proteins also acts synergistically on glycolysis (Fig. 5*C*). Still, only PRL-1/2 mainly affects glucose utilization for rapid energy demand as observed by changes in glycolytic reserve/capacity in their absence. These observations confirm a functional interplay between TRPM7 and PRL-1/2 to control bioenergetic needs.

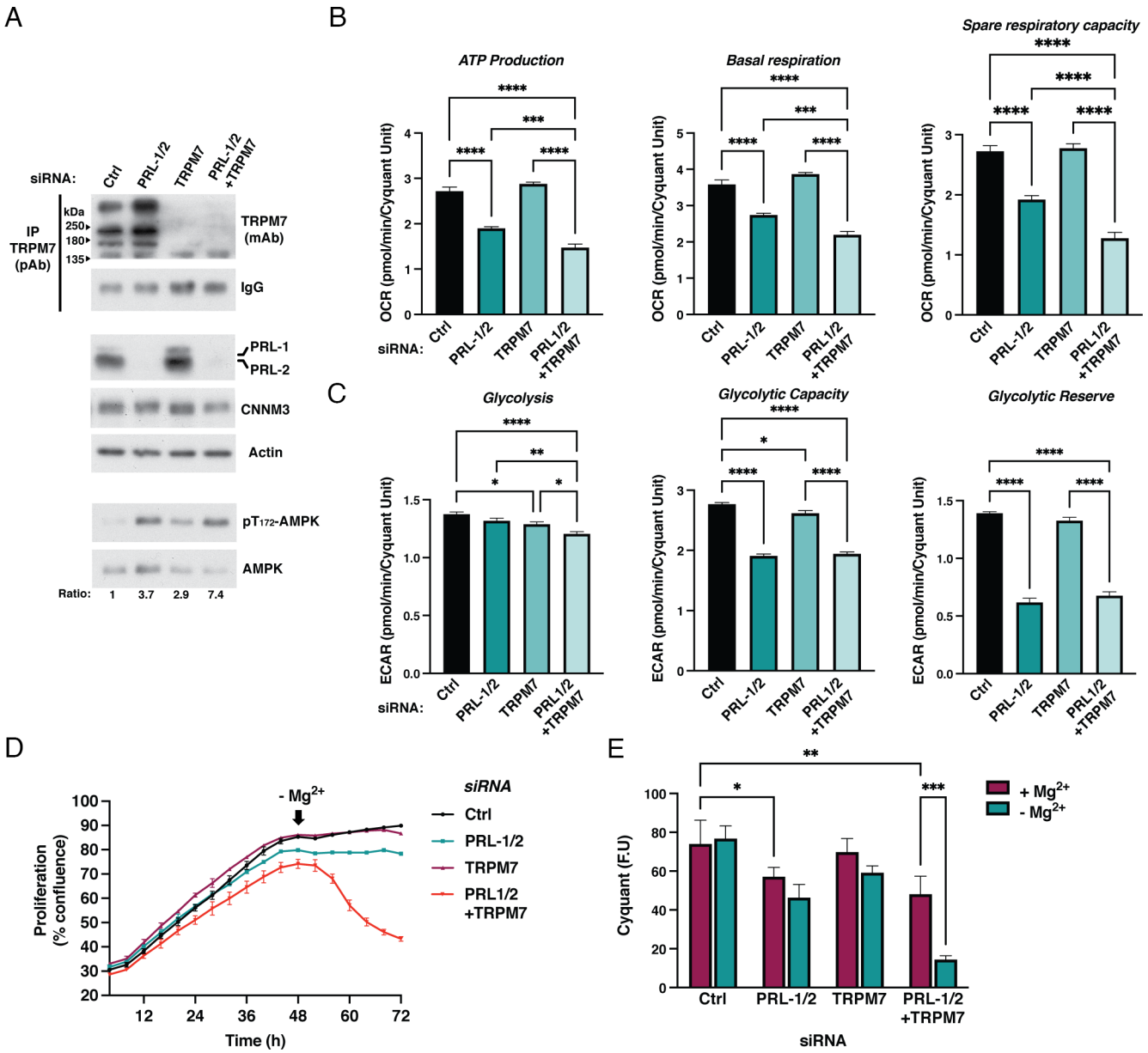

Fig. 5. TRPM7 and PRL activities synergize to control metabolic adaptation and cell fate. (*A*) MCF-7 cells were transfected with control, TRPM7, or PRL-1/2-targetting siRNAs for 48 h. Western blot analysis was performed following TRPM7 immunoprecipitation (IP) or on total cell lysates. Ratio of p-AMPK/AMPK is indicated. pAb: polyclonal antibody; mAb: monoclonal antibody. (*B* and *C*) MCF-7 cells were transfected as (*A*) followed by bioenergetics profiling of the mitochondrial function (*B*) and glycolytic activity of the cells (*C*). OCR: oxygen consumption rate; ECAR: extracellular acidification rate. Plot is representative of three independent experiments. Data are means ± SD (n = 8); ****$P < 0.0001$; ***$P < 0.001$; **$P < 0.01$; *$P < 0.05$ by two-way ANOVA. (*D* and *E*) MCF-7 cells were transfected with control, TRPM7, or PRL-1/2-targetting siRNAs, and proliferation was measured in real time (*D*) or at 72 h (*E*). Arrow indicates that magnesium was depleted ($-Mg^{2+}$) 48 h posttransfection. Plots are representative of three independent experiments. Data are means ± SD (n = 4); ***$P < 0.001$; **$P < 0.01$; *$P < 0.05$ by two-way ANOVA.

In line with this, PRL-1/2 ablation decreases proliferation in the presence of magnesium, whereas reduced TRPM7 expression has no effect. However, while knockdown of both TRPM7 and PRL-1/2 affects proliferation in the presence of magnesium, lowering magnesium levels dramatically induces cell death (Fig. 4*D*). This is not observed when we knockdown these genes individually, indicating a synergistic detrimental effect when these cells are submitted to metabolic stress like magnesium depletion as they presumably cannot meet the bioenergetic requirements for cell survival. Overall, we establish that PRL-1/2 is critical for maintaining intracellular magnesium levels by a mechanism involving TRPM7 magnesium-dependent function. This is consistent with a regulatory role we describe for PRL-1/2 within the TRPM7/CNNM protein complex, whereby PRL-1/2 expression destabilizes this association to contribute to the metabolic rewiring of cells in order for them to meet bioenergetic needs.

Discussion

In this study, we have characterized a unique mechanism that regulate magnesium homeostasis by controlling the activity of TRPM7. First, we confirmed that the CNNM family of magnesium modulators interact with the TRPM7 magnesium channel, as was recently described (15, 16). Second, this interaction is significantly strengthened in the presence of the small GTPase ARL15, which we recently identified as an interacting partner of

all CNNM members that inhibits magnesium flux by modulating CNNMs N-glycosylation states (40). Third, all CNNMs appear to have an inhibitory effect on the activity of TRPM7 as a magnesium channel, its ability to affect cytoskeletal rearrangements, and its downstream signaling. Fourth, PRL-1/2 act as a magnesium biosensor to promote TRPM7 signaling by regulating the interaction between CNNM3 and TRPM7 in a magnesium-dependent manner. Taken together, these findings lead us to propose the following model: In the presence of abundant magnesium, CNNMs interact with TRPM7, and ARL15 enhances the interaction in order to inhibit magnesium uptake. To alleviate a reduction in magnesium, the cells respond in the following ways (Fig. 6): As PRL-1/2 expression rises, their interaction with CNNM3 also increases, which reduces binding between ARL15, CNNM3, and TRPM7. This process derepresses TRPM7 function to promote magnesium influx. This model can also explain previous observations whereby ARL15 decreases magnesium uptake (40) and PRL-1/2 increase it (3, 4), which is not by direct regulation of magnesium flux through CNNMs as was previously thought but instead via modulation of TRPM7 activity. Moreover, our model also accounts for the CNNM efflux mechanism previously described (49), whereby CNNM2 and CNNM4 overexpression reduces intracellular magnesium levels, which can also be the result of their inhibitory effect on TRPM7 as we propose here. Still, our data cannot exclude that some CNNM members can act as true magnesium transporters as previously suggested (50, 51).

Whether these interactions happen at the plasma membrane, or other intravesicular magnesium stores, is uncertain. TRPM7 is localized at the plasma membrane but is also abundant in specific intracellular vesicles where it releases zinc from those vesicles following zinc overload (23). In plants and fungi, various magnesium transporters are associated with vacuolar membranes and function in magnesium retrieval from the vacuole to the cytoplasm, thereby providing a mechanism for low magnesium conditions (52–54). Interestingly, MAM3, the yeast homolog of the CNNMs, functions specifically in vacuolar magnesium accumulation and is essential for tolerance to high magnesium (54). It is unclear whether magnesium can be similarly regulated in mammals. Still,

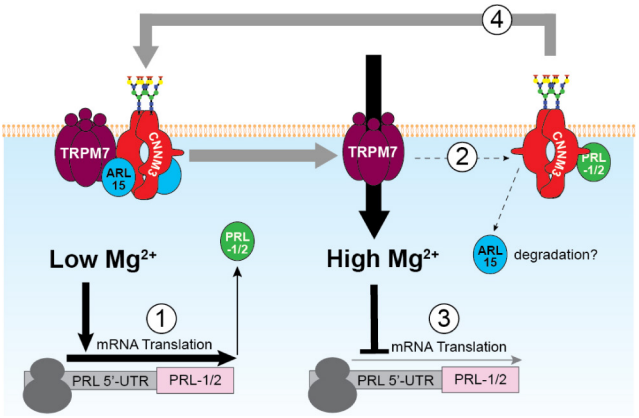

Fig. 6. Proposed mechanism for the control of TRPM7 Mg^{2+}-dependent activity. In the presence of abundant magnesium, TRPM7 interaction with CNNM is enhanced by ARL15, to reduce its activity. When cells require magnesium for specific cellular processes (e.g., metabolism, proliferation, cell cycle) or in low magnesium condition (e.g., tumor microenvironment), cells respond by: 1) increasing mRNA translation of PRL-1/2, thus promoting its interaction with CNNM3. Then, 2) the interaction between CNNM3 and ARL15 decreases, the latter being degraded, resulting in the derepression of TRPM7 activity, which increases magnesium influx. 3) When intracellular magnesium is repleted, PRL-1/2 expression is shut down, and 4) CNNM3 interaction with TRPM7 is restored.

in mammalian cells, the CNNMs localized to the plasma membrane and intracellular vesicles similarly to TRPM7 and the PRLs (15, 23, 24, 40, 55), suggesting that the interaction might not only be at the plasma membrane. Interestingly, our magnesium reporter described herein can also detect loss of mitochondrial magnesium, indicating that the signal obtained in our assay is not only representative of magnesium flux derived from the extracellular environment. Microscopic characterization of these multifaceted dynamic interactions with the four members will be a challenging task, given that overexpression or knockdown of each member affects the expression/stability of the others, as we show here, and that no suitable antibodies are available for immunofluorescence studies at endogenous levels.

Based on the PRL 5′UTR magnesium-sensing regulatory function (11), we developed a translationally regulated magnesium luminescence reporter to aid in the study of magnesium homeostasis. When magnesium is abundant, reporter activity is suppressed. In line with this, we demonstrate that induction of TRPM7 overexpression results in a dramatic decrease in luminescence. TRPM7 is a well-characterized divalent ion transporter and has previously been shown to increase intracellular magnesium levels when overexpressed (32, 41). Since TRPM7 is also known to transport calcium and zinc in addition to other divalent cations (17), we showed that the reporter activity can only be specifically modulated by magnesium. Here, we used this reporter to indirectly assess TRPM7 magnesium-dependent activity in a cellular model to examine the modulation of TRPM7 function by multiple interacting partners. Patch-clamp method has been widely considered the gold standard to directly record ion channel activity at the plasma membrane, including TRPM7. Still, TRPM7 is mainly present in intracellular vesicles inaccessible to patch-clamp recording using regular techniques (23, 24), indicating that other functions of TRPM7 may have been missed. We believe that the use of the reporter can circumvent this by measuring an overall response following TRPM7 activation. Also, most methods for detecting and quantifying intracellular magnesium rely on semi-specific magnesium chelators substituted with fluorophores (56). These traditional chelator-based reporters are challenging for prolonged measurements or measuring fluctuations of magnesium levels using in vivo models, thus making our reporter a unique candidate for these types of experiments. There have been efforts toward developing genetically encoded Mg^{2+} reporters (57, 58), and we trust that our first-generation magnesium biosensor is therefore an appealing candidate for the development of more sensitive genetically encoded Mg^{2+} reporters.

PRLs are involved in various biological processes and in the progression of multiple cancer types (1). Although substrates have been identified for the PRLs (59, 60), the importance of the PRL/CNNM complex in cancer development has also been established (3, 4, 9, 10), which highlights the potential role of magnesium in cancer growth. Likewise, TRPM7 is overexpressed in multiple cancers and is involved in their progression, which is dependent on magnesium in multiple cases (reviewed in ref. 61). In addition, TRPM7 is involved in the regulation of cellular morphology and cytoskeletal dynamics, which alters the proliferation and migration of cancer cells (25, 26). Thus, it would be informative to better understand the effect of TRPM7 on cancer progression via its regulation by the PRLs. Interestingly, in MCF-7 breast cancer cells, our data suggest that TRPM7 seems to play a more prominent role in glucose metabolism than mitochondrial respiration, suggesting a hypothetical role of TRPM7 in the Warburg effect (REF). Also, we showed that knocking down both PRL-1/2 and TRPM7 strongly reduced breast cancer cell proliferation and mitochondrial function, whereas knocking down TRPM7

individually had a lesser effect. This synergistic action of PRL-1/2 and TRPM7 on proliferation was enhanced in lower magnesium conditions, validating their cooperating function on magnesium homeostasis. Furthermore, we observed that upregulation of PRL-2 expression increases TRPM7 downstream signaling, while knockdown of PRL-1/2 dampens it. Interestingly, both TRPM7 and PRL-1/2 are rapidly coup-regulated at the mRNA translation level in response to magnesium depletion (11, 29), and we observe here that PRL-1/2 expression elicits a dose-dependent magnesium effect which also corresponds to reported extracellular magnesium concentrations modulating TRPM7 activity (36). As such, given that TRPM7 also transports zinc and calcium, we propose that PRL-1/2 primarily control their magnesium channel activity. In bacteria, the PhoP/PhoQ two-component system governs magnesium homeostasis by a mechanism involving the 5′UTR of various proteins involved in magnesium transport, which functions as a magnesium-sensing device or riboswitch (62). We believe that PRL-1/2 could act in a similar manner in vertebrates to dictate the response by the TRPM7/CNNM complexes. Under low magnesium, PRL-1/2 mRNA translation is rapidly increased by a mechanism involving the magnesium-sensitive uORF located in its 5′UTR (1), which leads to PRL-1/2 association with CNNMs, and TRPM7 activation to replenish intracellular magnesium. Taken together, our observations strongly suggest that PRL-1/2 and TRPM7 cooperate to maintain magnesium homeostasis.

Kollewe et al. showed that TRPM7 interacts with all CNNMs, and using overexpression systems, that ARL15 but not CNNM3, inhibits TRPM7 channel activity by patch-clamp assay (16). Also, Bai et al. confirmed the interactions between TRPM7 and all CNNMs, but they showed that CNNMs have a dual function: They activate, rather than inhibit, TRPM7 divalent cation influx activity while they themselves directly increase magnesium efflux activity, also using overexpression systems or stable knockout cells (15). This group also showed that increasing the ARL15 level decreases TRPM7-mediated zinc influx, while overexpression of the three PRLs has an opposite effect. The results of these two papers are difficult to reconcile since they diverge on the effects of CNNMs on TRPM7 activity while agreeing on the effect of ARL15 function. Additionally, our reporter assay data do not correspond with these publications as we show that CNNMs alone inhibit TRPM7 function, and this inhibitory effect is enhanced by ARL15. Given the magnesium ion specificity of our reporter, we could reason that we are only looking at the magnesium-dependent activity of TRPM7. Still, these disagreements reinforce the challenges of studying magnesium transport regulation using TRPM7 overexpression systems or using modified stable cell lines where cellular adaptation occurs. Therefore, further study at the endogenous level is crucial to studying TRPM7 function. Here, we provide a step in this direction by validating the regulation of endogenous TRPM7/CNNM protein complex formation by endogenous PRL-1/2 via the modulation of TRPM7 activity through alterations of extracellular magnesium levels.

While two recent papers on the structure of archaeal and bacterial homologs of CNNMs point toward their ability to transport magnesium (50, 51), they do not invalidate the possibility of mammalian CNNMs acting as magnesium sensors. Eukaryotic CNNM3 lacks the residues necessary for magnesium coordination that were found in prokaryotic homologs and yet it can regulate TRPM7-magnesium dependent function. Still, our data cannot exclude that CNNMs could act as both TRPM7 regulators and genuine magnesium transporters as proposed by Kollewe et al. (16).

Overall, we describe a unique layer of magnesium homeostasis through dynamic interactions between the magnesium channel TRPM7 and CNNM magnesium transport mediators, fine-tuned by PRL-1/2. The precise mechanism of TRPM7 channel regulation by magnesium is still not well understood. Here, we propose that CNNM3 acts an as inhibitor of TRPM7 function, and that the interaction between CNNM3 and TRPM7 is regulated by PRL-1/2 in a magnesium-dependent fashion. We believe that the dynamic change of this protein complex in response to magnesium levels could explain how TRPM7 function is regulated.

Materials and Methods

Cell Lines and Cell Culture. MCF-7, HEK293, and HeLa were initially obtained from the American Type Culture Collection. HEK293 dox-inducible HA-TRPM7 WT and K1646R cell lines has been previously described (39). All cell lines were cultured in high-glucose Dulbecco's Modified Eagle Medium (DMEM) (Fisher Scientific, #SH30081.01) supplemented with 10% fetal bovine serum (FBS) (Thermo Fisher Scientific) and 1% gentamicin (Wisent Bioproducts, #450-135-XL). Where indicated, magnesium-free DMEM (Wisent) and dialyzed FBS (Thermo Fisher Scientific) were used to vary the concentrations of magnesium by the addition of MgSO4 which is about 1 mM in regular DMEM. Where stated, the following concentrations of inhibitors were used: actinomycin D (1 μg/mL), CHX (50 μg/mL), MG132 (5 μM), NS8593 (20 μM), and TPEN (5 μM). For experiments with cation exclusion, custom high-glucose DMEM without magnesium, calcium, was used (Wisent Bioproducts, #319- 129-CL) in the presence of dialyzed FBS. It was supplemented with MgSO4 (1 mM), CaCl2 (1.8 mM), ZnCl2 (10 μM), CuCl2 (10 μM), MnCl2 (20 nM), CoCl2 (10 nM), and NiCl2 (10 nM). Cells were tested for *mycoplasma* contamination by PCR. All cell lines were maintained at 37 °C in a 5% CO2 incubator.

Generation of Magnesium-Sensitive Reporter Plasmid Constructs. A DNA fragment consisting of the CMV immediate enhancer/β-actin (CAG) promoter upstream of a multiple cloning site (MCS) and polyadenylation (pA) tail sequence was generated by overlap PCR and cloned into pZDonor-AAVS1 puromycin vector (Sigma Aldrich) using SLiCE cloning to first generate the pZDONR CAG-MCS-pA plasmid. Then, the magnesium reporter construct was created by cloning PRL-2 5′UTR (11) upstream of Fluc (luc2), with or without destabilizing sequence, amplified from CMV-LUC2CP/ARE plasmid (Addgene #62857). PRL-2 5′UTR luciferase fragments were cloned into pZDONR CAG-MCS-pA vector using SLiCE cloning to generate pZDonor-UTR-Luc and pZDonor-UTR-LucCP. Control vectors were cloned in a similar way without the inclusion of the UTR.

Plasmid Constructs. The following constructs were previously described: human FLAG-tagged pDEST26- CNNM1-4 and FLAG-tagged ARL15 (40), V5-tagged wild-type CNNM3 (9), and GST-PRL-2 (46). V5-tagged ARL15 was obtained from the McGill Platform for Cellular Perturbation cloned into pLX317 plasmid.

Transfection and Generation of Stable Cell Lines. Transfection was performed with Lipofectamine 2000 (Invitrogen) for protein overexpression at 1:2 (μg DNA:μL Lipofectamine) or Lipofectamine RNAiMAX (Invitrogen) for siRNA at 4:1 (nM siRNA:μL Lipofectamine). Dharmacon siRNA smart pools were purchased from Horizon for knockdown of PRL-1, PRL-2, TRPM7, and nontargeting control. Where indicated, HA-TRPM7 expression was induced with 1 μg/mL dox (Sigma-Aldrich). To generate stable cell lines, pZDonor-UTR-LucCP construct and lentiCRISPR v2 (Addgene #52961) containing sgRNA targeting the AAVS1 locus (ATCCTGTCCCTAGTGGCCC) were transfected in HeLa and HEK293 dox-inducible HA-TRPM7 WT cells using Lipofectamine 2000 as described above. Puromycin antibiotic selection was performed followed by single clone expansion.

Luciferase Assay. Reverse transfection was performed with 50 ng DNA and 0.1 μL Lipofectamine 2000 in 10 μL OptiMEM per well in a 96-well plate. 5,000 to 40,000 HeLa, HEK293, or HEK293 dox-inducible HA-TRPM7 cells in 90 μL of complete media were added to each well and incubated overnight. The media was then replaced according to the experiment performed or dox was added to induce TRPM7 expression for 24 h. The Fluc activity was normalized relative to the activity of the cotransfected pRL vector (Promega) expressing Renilla luciferase (Rluc) using the Dual Luciferase Stop and Glo Reporter assay system (Promega) and expressed as a ratio of Fluc/Rluc signal. Also, Fluc activity alone was determined

using One-glo assay system (Promega) (See Dataset S1 for statistical analysis). For live luciferase measurements, cells were incubated in the indicated media containing 100 μM D-luciferin. The 96-well plate was sealed with clear adhesive tape and the luminescence readings were collected every 10 min for 24 h using a SpectraMax i3 (Molecular Devices) plate reader set at 37 °C.

Cell Confluency Analysis. Reverse transfection in HEK293 dox-inducible HA-TRPM7 cells was performed as described above for the luciferase assay in a 96-well plate. For MCF-7 cells, reverse transfection was performed using 2 pmole siRNA and 0.2 μL Lipofectamine RNAiMAX in 10 μL OptiMEM per well in a 96-well plate followed by the addition of 2,500 cells in 90 μL of complete media. The plates were then placed inside IncuCyte ZOOM system with a 4X objective. Photographs of wells were taken every 2 h and then analyzed in the IncuCyte software to measure cell confluence.

Western Blot and Immunoprecipitation. Western blotting was done as described previously (11). The following antibodies were used: PRL-1/2 (Sigma-Aldrich #05-1583), CNNM3 (Proteintech #13976-1-AP), HA (Cell Signaling #3724), FLAG (Cell Signaling #14793), pS235/236 S6 (Cell Signaling #4858), pS240/244 S6 (Cell Signaling #2215), S6 (Cell Signaling #2317), pERK1/2 (Cell Signaling #4376S), ERK1/2 (Cell Signaling #4695), actin (Sigma-Aldrich #A3853), V5 (Life Technologies #R96025), and TRPM7 (mAb Stressmarq SMC-316). For immunoprecipitation proteins, cells were lysed in a mild immunoprecipitation (IP) lysis buffer containing 150 mM NaCl, 20 mM Tris, 1% Triton X-100 at pH 7.5. Anti-FLAG (Sigma-Aldrich #M8823) or anti-HA (Fisher Scientific #88836) magnetic beads were used to immunoprecipitate tagged proteins. The beads were washed and preblocked with 5% BSA for 1 h on a rotator at 4 °C. Protein lysates were precleared with agarose beads (Agarose Bead Technologies #A-1040S-500) for 1 h on a rotator at 4 °C. The precleared lysates and preblocked beads were then mixed and incubated on a rotator for at least 2 h at 4 °C. After incubation, beads were washed five times with the IP lysis buffer. 2X Laemmli buffer with 2-mercaptoethanol (Life Technologies) was added to the beads after washing and subjected to western blotting. For endogenous TRPM7 or CNNM3 immunoprecipitation, protein lysates were incubated with rabbit polyclonal anti-TRPM7 (Abcam 262698), anti-TRPM7 (mAb Stressmarq SMC-316), or anti-CNNM3 (Proteintech #13976-1-AP) with Protein A or G magnetic beads (ThermoFisher) for 24 h and then processed as described above. All western blots are representative of at least three independent experiments.

Extracellular Flux Analyzer. Metabolic changes of oxygen consumption rate (OCR) and extracellular acidification rate (ECAR) were measured using Seahorse XFe96 extracellular flux analyzers. MCF-7 cells were transfected with siRNAs directly in the XF96 microplates as described above for the Incucyte assay and incubated in a 5% CO_2 incubator at 37 °C for 48 h. For the assay itself, 50 μL of media was carefully removed from the wells using a multichannel pipette, cells were gently washed twice with XF assay medium, and fresh XF assay medium was added. The plate was incubated for one hour in a CO_2-free incubator at 37 °C for the equilibration period. The cell plate was then transferred to the XFe96 extracellular flux analyzer and the assay was performed, where one cycle consisted of a 2-min mix, 2-min wait, and 3-min measure period. Four cycles were performed at basal level and after injection of each drug. To measure mitochondrial respiration, oligomycin (1.5 μM), FCCP (0.5 μM), and rotenone/antimycin A (1 μM) were added at specific time points to inhibit different complexes of the ETC. For the glycolytic assays, glucose (10 mM), oligomycin (1.5 μM), and 2-deoxy-D-glucose (2-DG) (100 mM) were injected at a final concentration of 10 mM, 1.5 μM, and 100 mM, respectively. Each assay was performed with at least eight replicates and normalized to cell number by performing a CyQUANT assay, as per manufacturer's recommendations.

Data, Materials, and Software Availability. All study data are included in the article and/or *SI Appendix*.

ACKNOWLEDGMENTS. This work was supported by Canadian Institutes of Health Research (CIHR) Grants (FDN-159923) and by a grant from Fonds de recherche du Québec-Santé FRQ-S #294027 and by a grant from the CIHR ERT-168503, under the frame of E-Rare-3, the ERA-Net for Research on Rare Diseases. In addition, this project has received funding from the European Union's Horizon 2020 research and innovation program under the EJP RD COFUND-EJP No. 825575. We would like to thank Dr. Teri Hatzihristidis (NIH, Bethesda, USA) for constructive criticism and proofreading of the manuscript. M.L.T. is a Jeanne and Jean-Louis Lévesque Chair in Cancer Research and holds a Distinguished James McGill Chair from McGill University. J.C. is a recipient of Elizabeth Steffen Memorial Studentship training award. Y.Z. is a recipient of doctoral training award from Fonds de Recherche Santé Quebec.

Author affiliations: [a]Goodman Cancer Institute, McGill University, Montreal, QC H3A1A3, Canada; and [b]Department of Biochemistry, McGill University, Montreal, QC H3A1A3, Canada

1. S. Hardy *et al.*, Physiological and oncogenic roles of the PRL phosphatases. *FEBS J.* **285**, 3886–3908 (2018).
2. M. Wei, K. V. Korotkov, J. S. Blackburn, Targeting phosphatases of regenerating liver (PRLs) in cancer. *Pharmacol. Ther.* **190**, 128–138 (2018).
3. S. Hardy *et al.*, The protein tyrosine phosphatase PRL-2 interacts with the magnesium transporter CNNM3 to promote oncogenesis. *Oncogene* **34**, 986–995 (2015).
4. Y. Funato *et al.*, Membrane protein CNNM4-dependent Mg2+ efflux suppresses tumor progression. *J. Clin. Invest.* **124**, 5398–5410 (2014).
5. P. Gimenez-Mascarell *et al.*, Current structural knowledge on the CNNM family of magnesium transport mediators. *Int. J. Mol. Sci.* **20**, 1135 (2019).
6. J. H. de Baaij *et al.*, Membrane topology and intracellular processing of cyclin M2 (CNNM2). *J. Biol. Chem.* **287**, 13644–13655 (2012).
7. G. A. C. Franken *et al.*, The phenotypic and genetic spectrum of patients with heterozygous mutations in cyclin M2 (CNNM2). *Hum. Mutat.* **42**, 473–486 (2021).
8. D. A. Parry *et al.*, Mutations in CNNM4 cause Jalili syndrome, consisting of autosomal-recessive cone-rod dystrophy and amelogenesis imperfecta. *Am. J. Hum. Genet.* **84**, 266–273 (2009).
9. E. Kostantin *et al.*, Inhibition of PRL-2.CNNM3 protein complex formation decreases breast cancer proliferation and tumor growth. *J. Biol. Chem.* **291**, 10716–10725 (2016).
10. G. Kozlov *et al.*, PRL3 pseudophosphatase activity is necessary and sufficient to promote metastatic growth. *J. Biol. Chem.* **295**, 11682–11692 (2020).
11. S. Hardy *et al.*, Magnesium-sensitive upstream ORF controls PRL phosphatase expression to mediate energy metabolism. *Proc. Natl. Acad. Sci. U.S.A.* **116**, 2925–2934 (2019).
12. G. A. C. Franken, M. A. Huynen, L. A. Martinez-Cruz, R. J. M. Bindels, J. H. F. de Baaij, Structural and functional comparison of magnesium transporters throughout evolution. *Cell. Mol. Life Sci.* **79**, 418 (2022).
13. F. J. Arjona, J. H. F. de Baaij, CrossTalk opposing view: CNNM proteins are not Na(+) /Mg(2+) exchangers but Mg(2+) transport regulators playing a central role in transepithelial Mg(2+) (re) absorption. *J. Physiol.* **596**, 747–750 (2018).
14. Y. Funato, K. Furutani, Y. Kurachi, H. Miki, CrossTalk proposal: CNNM proteins are Na(+) /Mg(2+) exchangers playing a central role in transepithelial Mg(2+) (re)absorption. *J. Physiol.* **596**, 743–746 (2018).
15. Z. Bai *et al.*, CNNM proteins selectively bind to the TRPM7 channel to stimulate divalent cation entry into cells. *PLoS Biol.* **19**, e3001496 (2021).
16. A. Kollewe *et al.*, The molecular appearance of native TRPM7 channel complexes identified by high-resolution proteomics. *Elife* **10**, e68544 (2021).
17. V. Chubanov, L. Mittermeier, T. Gudermann, Role of kinase-coupled TRP channels in mineral homeostasis. *Pharmacol. Ther.* **184**, 159–176 (2018).
18. L. Mittermeier *et al.*, TRPM7 is the central gatekeeper of intestinal mineral absorption essential for postnatal survival. *Proc. Natl. Acad. Sci. U.S.A.* **116**, 4706–4715 (2019).
19. L. V. Ryazanova *et al.*, TRPM7 is essential for Mg(2+) homeostasis in mammals. *Nat. Commun.* **1**, 109 (2010).
20. J. Jin *et al.*, The channel kinase, TRPM7, is required for early embryonic development. *Proc. Natl. Acad. Sci. U.S.A.* **109**, E225–E233 (2012).
21. Y. Komiya, L. W. Runnels, TRPM channels and magnesium in early embryonic development. *Int. J. Dev. Biol.* **59**, 281–288 (2015).
22. G. Krapivinsky, L. Krapivinsky, Y. Manasian, D. E. Clapham, The TRPM7 chanzyme is cleaved to release a chromatin-modifying kinase. *Cell* **157**, 1061–1072 (2014).
23. S. A. Abiria *et al.*, TRPM7 senses oxidative stress to release Zn(2+) from unique intracellular vesicles. *Proc. Natl. Acad. Sci. U.S.A.* **114**, E6079–E6088 (2017).
24. M. S. Schappe *et al.*, Efferocytosis requires periphagosomal Ca(2+)-signaling and TRPM7-mediated electrical activity. *Nat. Commun.* **13**, 3230 (2022).
25. S. Luanpitpong *et al.*, A novel TRPM7/O-GlcNAc axis mediates tumour cell motility and metastasis by stabilising c-Myc and caveolin-1 in lung carcinoma. *Br. J. Cancer* **123**, 1289–1301 (2020).
26. X. Y. Cheng *et al.*, Transient receptor potential melastatin 7 and their modulators. *Eur. J. Pharmacol.* **931**, 175180 (2022).
27. E. Oancea, J. T. Wolfe, D. E. Clapham, Functional TRPM7 channels accumulate at the plasma membrane in response to fluid flow. *Circ. Res.* **98**, 245–253 (2006).
28. C. L. Yankaskas *et al.*, The fluid shear stress sensor TRPM7 regulates tumor cell intravasation. *Sci. Adv.* **7**, eabh3457 (2021).
29. I. A. Nikonorova, N. V. Kornakov, S. E. Dmitriev, K. S. Vassilenko, A. G. Ryazanov, Identification of a Mg2+-sensitive ORF in the 5'-leader of TRPM7 magnesium channel mRNA. *Nucleic Acids Res.* **42**, 12779–12788 (2014).
30. R. Chokshi, M. Matsushita, J. A. Kozak, Sensitivity of TRPM7 channels to Mg2+ characterized in cell-free patches of Jurkat T lymphocytes. *Am. J. Physiol. Cell Physiol.* **302**, C1642–C1651 (2012).
31. E. Schmidt *et al.*, Structural mechanism of TRPM7 channel regulation by intracellular magnesium. *Cell. Mol. Life Sci.* **79**, 225 (2022).

32. M. J. Nadler *et al.*, LTRPC7 is a Mg.ATP-regulated divalent cation channel required for cell viability. *Nature* **411**, 590–595 (2001).
33. J. H. de Baaij, J. G. Hoenderop, R. J. Bindels, Magnesium in man: Implications for health and disease. *Physiol. Rev.* **95**, 1–46 (2015).
34. C. C. Daw *et al.*, Lactate elicits ER-mitochondrial Mg(2+) dynamics to integrate cellular metabolism. *Cell* **183**, 474–489.e17 (2020).
35. N. Uetani *et al.*, PRL2 links magnesium flux and sex-dependent circadian metabolic rhythms. *JCI Insight* **2**, e91722 (2017).
36. A. Mellott *et al.*, TRPM7 channel activity in Jurkat T lymphocytes during magnesium depletion and loading: Implications for divalent metal entry and cytotoxicity. *Pflugers Arch.* **472**, 1589–1606 (2020).
37. T. Kubota *et al.*, Mitochondria are intracellular magnesium stores: Investigation by simultaneous fluorescent imagings in PC12 cells. *Biochim. Biophys. Acta* **1744**, 19–28 (2005).
38. R. Yamanaka *et al.*, Mitochondrial Mg(2+) homeostasis decides cellular energy metabolism and vulnerability to stress. *Sci. Rep.* **6**, 30027 (2016).
39. C. Schmitz *et al.*, Regulation of vertebrate cellular Mg2+ homeostasis by TRPM7. *Cell* **114**, 191–200 (2003).
40. Y. Zolotarov *et al.*, ARL15 modulates magnesium homeostasis through N-glycosylation of CNNMs. *Cell. Mol. Life Sci.* **78**, 5427–5445 (2021).
41. L. W. Runnels, L. Yue, D. E. Clapham, TRP-PLIK, a bifunctional protein with kinase and ion channel activities. *Science* **291**, 1043–1047 (2001).
42. V. Chubanov, T. Gudermann, Mapping TRPM7 function by NS8593. *Int. J. Mol. Sci.* **21**, 7017 (2020).
43. L. T. Su *et al.*, TRPM7 regulates cell adhesion by controlling the calcium-dependent protease calpain. *J. Biol. Chem.* **281**, 11260–11270 (2006).
44. J. Sahni, A. M. Scharenberg, TRPM7 ion channels are required for sustained phosphoinositide 3-kinase signaling in lymphocytes. *Cell Metab.* **8**, 84–93 (2008).
45. E. Gout, F. Rebeille, R. Douce, R. Bligny, Interplay of Mg2+, ADP, and ATP in the cytosol and mitochondria: Unravelling the role of Mg2+ in cell respiration. *Proc. Natl. Acad. Sci. U.S.A.* **111**, E4560–4567 (2014).
46. S. Hardy, N. N. Wong, W. J. Muller, M. Park, M. L. Tremblay, Overexpression of the protein tyrosine phosphatase PRL-2 correlates with breast tumor formation and progression. *Cancer Res.* **70**, 8959–8967 (2010).
47. P. Lujan *et al.*, PRL-3 disrupts epithelial architecture by altering the post-mitotic midbody position. *J. Cell Sci.* **129**, 4130–4142 (2016).
48. B. N. Desai *et al.*, Cleavage of TRPM7 releases the kinase domain from the ion channel and regulates its participation in Fas-induced apoptosis. *Dev. Cell* **22**, 1149–1162 (2012).
49. Y. Hirata, Y. Funato, Y. Takano, H. Miki, Mg2+-dependent interactions of ATP with the cystathionine-beta-synthase (CBS) domains of a magnesium transporter. *J. Biol. Chem.* **289**, 14731–14739 (2014).
50. Y. Huang *et al.*, Structural basis for the Mg(2+) recognition and regulation of the CorC Mg(2+) transporter. *Sci. Adv.* **7**, eabe6140 (2021).
51. Y. S. Chen *et al.*, Crystal structure of an archaeal CorB magnesium transporter. *Nat. Commun.* **12**, 4028 (2021).
52. S. F. Meng *et al.*, Four plasma membrane-localized MGR transporters mediate xylem Mg(2+) loading for root-to-shoot Mg(2+) translocation in Arabidopsis. *Mol. Plant* **15**, 805–819 (2022).
53. N. P. Pisat, A. Pandey, C. W. Macdiarmid, MNR2 regulates intracellular magnesium storage in Saccharomyces cerevisiae. *Genetics* **183**, 873–884 (2009).
54. R. J. Tang *et al.*, Conserved mechanism for vacuolar magnesium sequestration in yeast and plant cells. *Nat. Plants* **8**, 181–190 (2022).
55. Q. Zeng *et al.*, Prenylation-dependent association of protein-tyrosine phosphatases PRL-1, -2, and -3 with the plasma membrane and the early endosome. *J. Biol. Chem.* **275**, 21444–21452 (2000).
56. T. S. Lazarou, D. Buccella, Advances in imaging of understudied ions in signaling: A focus on magnesium. *Curr. Opin. Chem. Biol.* **57**, 27–33 (2020).
57. L. H. Lindenburg, J. L. Vinkenborg, J. Oortwijn, S. J. Aper, M. Merkx, MagFRET: The first genetically encoded fluorescent Mg2+ sensor. *PLoS One* **8**, e82009 (2013).
58. K. Maeshima *et al.*, A transient rise in free Mg(2+) ions released from ATP-Mg hydrolysis contributes to mitotic chromosome condensation. *Curr. Biol.* **28**, 444–451.e6 (2018).
59. V. McParland *et al.*, The metastasis-promoting phosphatase PRL-3 shows activity toward phosphoinositides. *Biochemistry* **50**, 7579–7590 (2011).
60. Q. Li *et al.*, Mechanism of PRL2 phosphatase-mediated PTEN degradation and tumorigenesis. *Proc. Natl. Acad. Sci. U.S.A.* **117**, 20538–20548 (2020).
61. S. Meng *et al.*, Role of TRPM7 kinase in cancer. *Cell Calcium* **96**, 102400 (2021).
62. E. A. Groisman, C. Chan, Cellular adaptations to cytoplasmic Mg(2+) Limitation. *Annu. Rev. Microbiol.* **75**, 649–672 (2021).